Available online at www.sciencedirect.com

ScienceDirect

Advances in Space Research 62 (2018) 2364–2371

ADVANCES IN SPACE RESEARCH (a COSPAR publication)

www.elsevier.com/locate/asr

Exospheric escape: A parametrical study

Rosemary M. Killen [a,*], Matthew H. Burger [b], William M. Farrell [a]

[a] NASA Goddard Space Flight Center, Code 695, 8800 Greenbelt Rd., Greenbelt, MD 20771, USA
[b] Space Telescope Science Institution, 3700 San Martin Dr., Baltimore, MD 21218, USA

Received 16 March 2017; received in revised form 25 May 2017; accepted 5 June 2017
Available online 27 June 2017

Abstract

The study of exospheres can help us understand the long-term loss of volatiles from planetary bodies due to interactions of planets, satellites, and small bodies with the interplanetary medium, solar radiation, and internal forces including diffusion and outgassing. Recent evidence for water and OH on the Moon has spurred interest in processes involving chemistry and sequestration of volatile species at the poles and in voids. In recent years, NASA has sent spacecraft to asteroids including Vesta and Ceres, and ESA sent Rosetta to comet 67P/Churyumov–Gerasimenko and the asteroids Lutetia and Steins. Japan's Hayabusa spacecraft returned a sample from asteroid Itakowa, and OSIRIS-REX will return a sample from a primitive asteroid, Bennu, to Earth. In a surface-bounded exosphere, the gases are derived from the surface and thus reflect the composition of the body's regolith, although not in a one-to-one ratio. Observation of an escaping exosphere, termed a corona, is challenging. We have therefore embarked on a parametrical study of exospheres as a function of mass of the exospheric species, mass of the primary body and source velocity distribution, specifically thermal (Maxwell-Boltzmann) and sputtering. The goal is to provide a quick look to determine under what conditions and for what mass of the primary body the species of interest are expected to be bound or escaping and to quickly estimate the observability of exospheric species. This work does not provide a comprehensive model but rather serves as a starting point for further study. These parameters will be useful for mission planning as well as for students beginning a study of planetary exospheres.
Published by Elsevier Ltd on behalf of COSPAR.

Keywords: Exospheres; Escape; Volatiles

1. Introduction

Surface-bounded exospheres, i.e., atmospheres that are collisionless down to an object's surface, are the most common type of atmosphere in the Solar System. They are known to occur at the Moon, Mercury, and several outer-planet moons. The primary mechanisms for these exospheres vary for different objects and exospheric species, but include micrometeoroid impact vaporization, photon-stimulated desorption, ion-sputtering, and thermal desorption. Several objects, such as Enceladus (Porco and the Cassini Imaging Team, 2006), Europa (Roth et al., 2014), and Ceres (Kuppers et al., 2014) show evidence of active venting of water.

Typical exospheric studies usually take a tactical approach, focusing on one component at one body (e.g., sodium at the Moon, etc.), providing detail on the source mechanism, species trajectory, and subsequent surface processes. However, general exospheric trends across body sizes and process temperatures or source velocity distributions have not been fully explored in a systematic way. In other fields, such parametric studies have proven to be very valuable, providing a general understanding of the controlling variables for use in predictions of the resulting effects. For example, impact parameter studies (Gault et al., 1972;

* Corresponding author.
E-mail address: rosemary.killen@nasa.gov (R.M. Killen).

http://dx.doi.org/10.1016/j.asr.2017.06.015
0273-1177/Published by Elsevier Ltd on behalf of COSPAR.

Housen and Holsapple, 2011) continue to provide insights on the impactor based on scalable cratering characteristics. An exosphere, although tenuous, may be gravitationally bound.

We have conducted a parametrical study of exospheres to distinguish between the bound and escaping components of exospheres (an escaping exosphere is commonly referred to as a corona). We describe a method for determining whether an exospheric species will gravitationally escape from a body as a function of the object radius and surface temperature, and the species mass and the source velocity distribution. We have considered Maxwellian velocity distributions at various temperatures and two sputter distributions, one consistent with sputtering from ices and one consistent with sputtering from regoliths. We do not consider specific source processes per se, but instead use the more general parameter of process temperature to identify a bounded vs. escaping exospheric component. We do not consider the subsequent interactions of released atoms or molecules with the surface for non-escaping species, since each interaction is specific to the atom/molecule and the surface. Despite the apparent limitations, the parametric study provides a scalable method to determine if a specific exosphere at a given body will remain primarily escaping or primarily bound – thereby identifying the body as a 'surface bounded exosphere'. Loss processes, such as photoionization, are not considered here.

2. Method

We assume that in a collisionless exosphere a neutral species escapes if it achieves escape velocity defined as:

$$v_{esc} = \left(\frac{2GM}{R}\right)^{1/2} = \left(\frac{8\pi}{3} G\rho R^2\right)^{1/2} \quad (1)$$

where G is the gravitational constant, R is the object radius, M is the object mass, and ρ is the object density.

For most processes, neutral species are ejected from the surface with a Maxwellian flux distribution in the form:

$$f(v) \propto v^3 \exp(-v^2/v_{th}^2) \quad (2)$$

where v_{th} is the thermal speed defined as $(2kT/m)^{1/2}$, k is Boltzmann's constant, T is the temperature, and m is the mass of the neutral species (Smith et al., 1978). The temperature could refer to the surface temperature, the temperature of the vapor cloud produced by impact vaporization, or other process that results in a thermal distribution (e.g., photon-stimulated desorption ejects Na with a ~1200 K Maxwellian distribution (Yakshinskiy and Madey, 2004).

We also consider a sputtering distribution in the form:

$$f(E) = \frac{EU^{\beta}}{(E+U)^{2+\beta}} \quad (3)$$

where U is the binding energy with the surface.

The sputtered flux $vf(v)$ would then be

$$vf(v) = vf(E)\frac{dE}{dv} \quad (4)$$

$$vf(v) \propto v^2 f(E(v)) \quad (5)$$

where

$$E \propto v^2 \quad (6)$$

and

$$U \propto v_{b0}^2 \quad (7)$$

Values of the binding energy, U, have been described as 0.052 eV consistent with sputtering from ice (Johnson et al., 2002) and 2–3 eV with sputtering from regolith (McGrath et al., 1986; Leblanc and Johnson, 2003), respectively. We have considered intermediate values of U as well. An empirical binding energy is often used for sputtering from planetary surfaces having been exposed to high fluences of charged particles resulting in chemically altered surfaces (Betz and Wehner, 1983; Roth, 1983). On planetary surfaces, an adsorbed layer, typically less than a monolayer in depth and bound more loosely than atoms in the crystalline lattice, can be desorbed by photons having energy of a few eV. The solar wind plasma energy, typically 1.5–10 keV, is deposited in the substrate and can therefore eject atoms from the crystalline lattice. Typical solar wind protons and ions have energy ~1 keV/AMU and penetrate tens of nm into the substrate (Barghouty et al., 2011). In addition to describing sputtering from icy bodies, the icy sputter velocity distribution (Eq. (3) with $\beta = 0.7$) has been used by some authors to simulate photon-stimulated desorption (e.g. Burger et al., 2010) because this velocity distribution is described by a cool core and a small extended tail (e.g. Yakshinskiy and Madey, 2000). For sputtering from rock, β in Eq. (3) is typically unity.

The fractional loss is given by

$$fracloss = \frac{\int_{vsec}^{\infty} vf(v)dv}{\int_{0}^{\infty} vf(v)dv} \quad (8)$$

3. Results

First we consider a Maxwell-Boltzmann flux distribution of particles (Eq. (2)) ejected from a body of radius, R, at temperature, T, for species of mass, m, in AMU (Smith et al., 1978). We show in Fig. 1 the temperature at which 50% of the ejected neutral species escape from a body as a function of the object radius and species mass. The body is assumed to have density 3.5 g cm^{-3}. A small body such as Phobos (radius = 11.27 km, v_{esc} = 11.39 m/s cannot hold any atmosphere at almost any temperature, whereas Earth-sized bodies are highly retentive for all gases except H, H_2, and He. Note that escape from an exobase at the top of an atmosphere is slightly different from escape from a surface-bounded exosphere (e.g. Chamberlain and

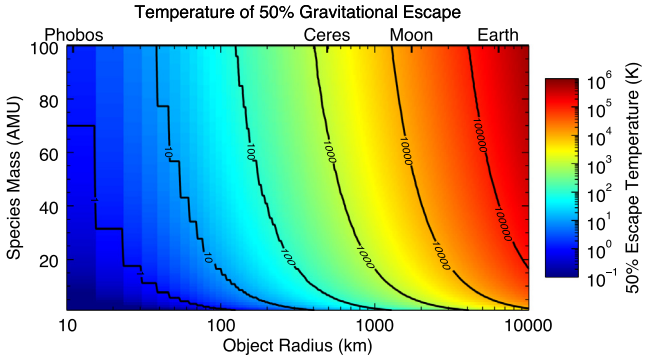

Fig. 1. The temperature at which 50% of an ejected neutral species escapes from a body (color-coded) is shown as a function of the object radius and species mass, assuming the body has a density of 3.5 g cm^{-3}. Because the mean densities of the planets and satellites vary this is only an approximation for the objects labeled at the top of the graph. A small body such as Phobos (radius = 11.27 km, v_{esc} = 11.39 m/s cannot hold any atmosphere at almost any temperature above 10 K.

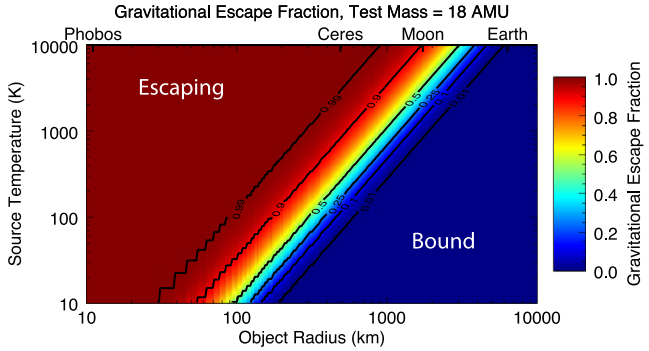

Fig. 2. The fraction of gas with mass 18 AMU (such as H_2O or CH_4) that escapes an object as a function of the object radius (again with a density assumption) and the temperature of the source process is shown. This assumes a Maxwell-Boltzmann flux at the base of the exosphere. For small bodies (<100 km), all the gas escapes regardless of temperature, whereas Earth-sized bodies retain all the water or methane for $T < 10{,}000$ K.

Hunten, 1987). Notably, the gravity at the exobase is reduced from that at the planet's surface.

Applying Fig. 1 for the Moon, it becomes clear that it takes an energetic surface process with an intrinsic temperature exceeding 10,000 K to force 50% of the adsorbed ^{40}Ar to fully escape from the Moon. Thus, ^{40}Ar release at the dawn terminator via thermal and photon-stimulated desorption creates simply a bounded outflow, as observed by LACE (Stern, 1999) and LADEE (Hodges and Mahaffy, 2016). In contrast, it takes a less energetic process, near 3000–4000 K, to result in 50% of OH and water (~18 AMU) escaping from the Moon. Such a process temperature is associated with micrometeoroid impacts. As such, we might expect up to 50% of water molecules mixed into the regolith of lunar polar cold traps and released by micro-meteoroids to escape from the Moon, and the other 50% to return in adjacent regions (Farrell et al., 2013, 2015).

We re-examine the escape of gas of mass ~18 AMU (OH, water, or methane) in a general way now as a function of exobase temperature and object radius. The Earth retains virtually all of its water gravitationally, whereas a body of radius 100 km or less retains almost none at temperatures greater than 100 K. This means that loss of water from Earth (or larger bodies) must be non-gravitational, such as via ionization, dissociation, chemistry or freezing or condensing to the surface. Note that Venus ($R = 6051$ km, $T_{surf} = 740$ K, $T_{cloud} = 230$ K) must have lost its water non-gravitationally unless temperatures at early times were >10,000 K. For bodies of intermediate size between Ceres and the Earth a varying range of water is gravitationally lost as shown in Fig. 2. The Moon's exosphere which has been under considerable study, has the 50% bounded/50% escaping fraction (the green and yellow line) pass through its radius near 3000–4000 K. Thus, energetic surface process will release the water with considerable escape while less energetic process such as thermal desorption will simply leave any water bounded. For small bodies (like Phobos), molecules near 18 AMU are unbounded (lost) even at low process temperatures (like 10 K).

Whereas for asteroids with $R < 100$ km all water is lost regardless of temperature at the exobase, and at the Earth ($R = 6371$ km) all water is retained even at 10,000 K, the Earth's moon is of intermediate size where the escape fraction is a strong function of temperature. Fig. 2 shows that an Earth-sized planet would retain water but escape from a Moon-sized body depends critically on details of the ejection process. Although details of escape are clearly different for an atmosphere, and water may be lost through photodissociation or ionization, one could surmise that water was not thermally lost on Earth even for the early times when a magma ocean may have been at 10,000 K, whereas the water escape rate at the Moon was 90% on each ballistic trajectory for the early Moon at 10,000 K. Even though currently the water escape rate at the Moon, even for a moderately energetic process such as photon-stimulated desorption - which produces ~1200 K ejecta - is only <5%, the escape fraction of water from impact vaporization on the Moon (~3000 K) is significant (also see Fig. 7).

One process that produces non-thermal gas is sputtering. Sputtering by ion-impact can occur at a surface or in an atmosphere. We consider here two sputter distributions: that produced by sputtering from a rock surface and that from an icy surface. The difference is mostly due to the binding energy that is required to overcome, which is about 2–3 eV in the case of rock and about 0.052 eV in the case of an icy surface. The velocity distributions are illustrated in Figs. 3 and 4. Note that the velocity is a function of the ejecta mass as well as binding energy. Although a continuum of binding energies is shown, for many of the elements discrete values of binding energy are expected. For others a continuum of binding energies may be found, especially on a space-weathered surface (e.g. Leblanc and Johnson, 2003; Poston et al., 2015). Hodges and Mahaffy (2016) found that

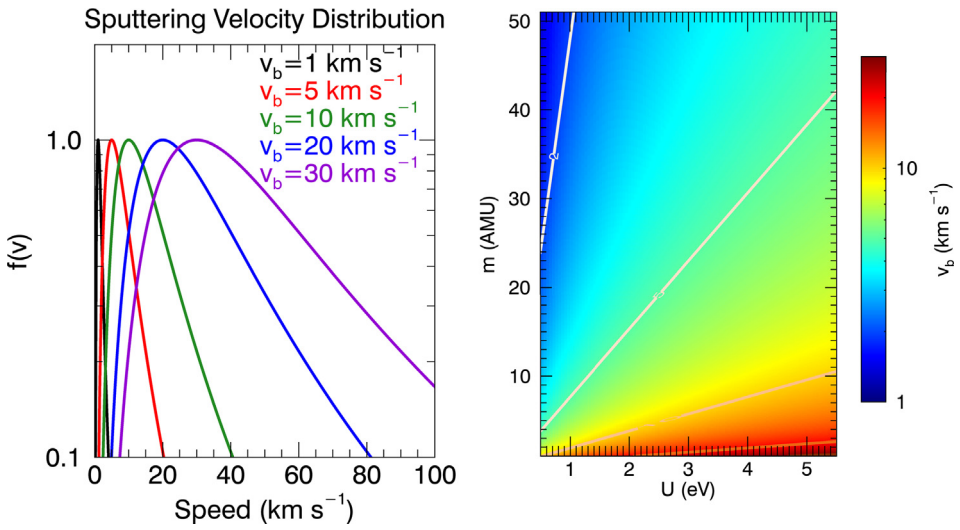

Fig. 3. The sputtering velocity distribution for sputtering from rock is shown as a function of the particle speed, where v_b is the velocity at peak of the distribution. V_b is a function of species mass and binding energy as shown in panel b. Light atoms like H and He have very high velocities for almost any binding energies; moderate velocities ($v_b \sim 5$ km/s) correspond to a wide range of masses depending on the binding energy at the surface. Heavy atoms like K and Ca are ejected at low velocities (~1 km/s) for $U < 2$ eV.

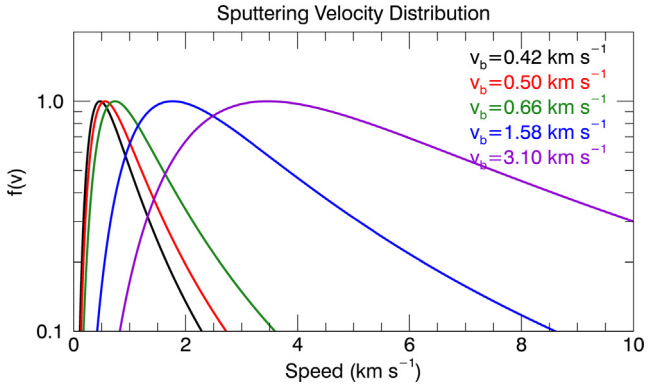

Fig. 4. This shows the velocity distribution for Eq. (3) with $\beta = 0.7$ and $U = 0.052$, consistent with sputtering from ice. The sputtering velocity distribution for a binding energy on ice of 0.052 eV indicates that the sputter ejection velocities will be relatively small. The plots are for Fe ($v_b = 0.42$), K ($v_b = 0.5$), Na ($v_b = 0.66$), He ($v_b = 1.58$) and H ($v_b = 3.1$ km/s). Very little of the ejecta of $m \geq 23$ AMU sputtered from ice (or with a 'cool sputter' distribution) would escape Mercury ($v_{esc} = 4.25$ km/s) and almost none for $m \geq 40$ AMU would escape the Moon ($v_{esc} = 2.38$ km/s). The velocity distribution of Na sputtered from an ice would be similar to that of thermal vaporization at the subsolar temperature of Mercury.

the adsorption energy of ^{40}Ar on the Moon varies almost linearly with temperature. Surface binding energies can be much higher for molecules of interest in planetary surfaces such as MgO and CaO (Kelly, 1987).

Fig. 5 reveals that >90% escape rate via the sputtering process from rock should be expected up to body sizes less than or comparable to the Moon for all species with mass <50 AMU. For body sizes larger than the Moon, there is increasing retention of sputtered atoms and molecules. For Earth-sized bodies, most species with mass greater than about 10 AMU are bounded. In this case, the region between completely bound and escaping is between Moon-sized and Earth-sized bodies. In the case of Maxwellian velocity distributions, the line delineating 50% bound and escaping for water is between Ceres-sized at 100 K and Moon-sized bodies at 4000 K. For bodies smaller than Ceres a mass 18 AMU particle will escape for most temperatures, whereas for bodies larger than the Moon a mass 18 particle will be retained for most temperatures. Thus it is most important to pay careful attention to conditions on bodies of these intermediate sizes when calculating thermal escape rates. Fig. 5 shows that objects the size of Mercury and greater retain most of the products more massive than sodium ejected with the icy sputter distribution (Fig. 5a), but even an Earth-sized exposed rocky body will lose more than half of ejecta sputtered from the rock even up to 50 AMU (Fig. 5b). This does not strictly apply to planets with a massive atmosphere. The range of radii (R) between 1000 km and 2500 km differentiates between escaping ($R < 1000$ km) and mostly bound ($R > 2500$ km) exospheres for the icy bodies, but for rocky bodies ($U > 2$ eV) the radii between 3000 and 6000 km differentiate between escaping ($R < 3000$ km) and partially bound ($R > 3000$ km). A comparison of Figs. 5 and 1 shows that the escape fraction of ^{40}K from an Earth-sized object via sputtering from rock would be ~40% whereas the escape fraction via a Maxwellian velocity distribution is 50% from an Earth-sized object at 100,000 K. This may explain why sputtered atoms are difficult to measure since their densities would be low. The equivalent temperature derived for the Ca escaping Mercury was estimated to be >70,000 K, consistent with sputter. Sputtering was rejected as a source process on the basis of its spatial distribution being inconsistent with open magnetic field lines.

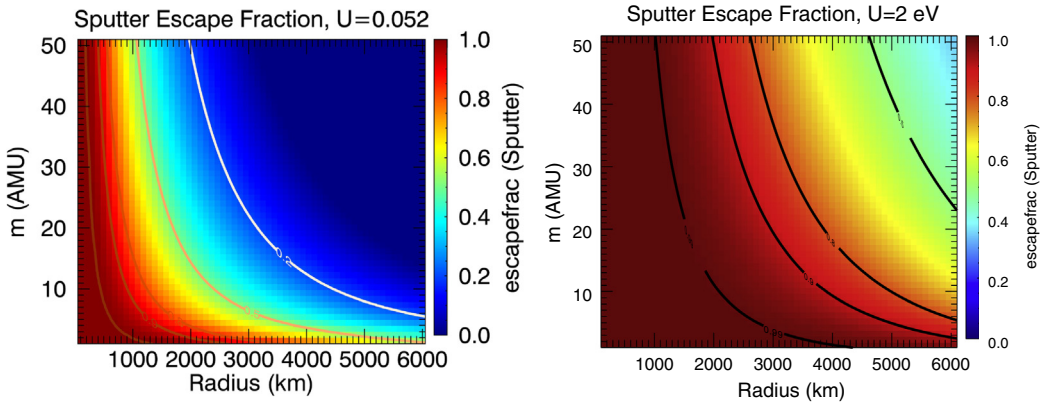

Fig. 5. The escape fraction is shown as a function of object radius and species mass, m, for a sputter distribution appropriate for sputtering from an icy body ($U = 0.052$ eV) (a) and that for a rocky surface ($U = 2$ eV) (b).

4. Specific studies

We have investigated three specific cases of interest: water at Ceres, OH at the Moon and oxygen at Mercury. The parameters appropriate for these cases are given in Table 1.

4.1. Water at Ceres

A'Hearn and Feldman (1992) observed sporadic OH over the northern pole of Ceres, possibly consistent with a northern polar cap of water frost. The velocity of OH from dissociation of H_2O is 1.1 km/s, is twice Ceres' escape velocity and therefore certainly escaping. They concluded that this is not consistent with infalling OH from meteorites but must be endogenous. The Visible and InfraRed (VIR) mapping spectrometer onboard the Dawn spacecraft detected water absorption features in Oxo crater, consistent with water ice and mineral hydrates (Combe et al., 2016). Kuppers et al. (2014) concluded that measured velocities of water at Ceres are consistent with thermal sublimation, and that most of the water does not come from the polar region. Landis et al. (2017) also considered ice sublimation as a source of the observed water vapor, but concluded that the exposed surface ice reported in Oxo crater by Combe et al. (2016) is an insufficient source, and showed that the sublimation rate of exposed surface ice at Ceres varies significantly throughout the Ceresian year. Villarreal et al. (2017) concluded that the cerean exosphere is correlated with the presence of solar energetic protons at Ceres, which may indicate that the ejection process is sputtering.

Given that the lifetime of H_2O against photodissociation at the orbit of Ceres is 6.6 days, and water thermally vaporized at surface temperatures <200 K is likely to stick to the surface, less than 16% of the water will dissociate on each ballistic trajectory of the water molecule (with a ballistic lifetime of about one hour). Water that thermally vaporizes may accumulate on the surface in cold traps. We show here the escape fractions of water at Ceres for thermal (Maxwell-Boltzmann) velocity distribution and for sputtering.

Fig. 6a and b compare water escape rates at Ceres for impact vaporization and sputtering for moderate binding energies. Impact vaporization over a region containing water will produce a rapidly escaping corona at about 1 km/s. None of this water will return to the surface. On the other hand 40–60% of water thermally vaporizing at the surface temperature ($T < 200$ K) will escape. Given that only a small fraction of the surface of Ceres may have exposed water ice, very little water is expected to accumulate on the surface but it could accumulate near its source.

The escape fraction of water sputtered from icy patches on Ceres is >0.97 assuming Eq. (3) with a binding energy, U, of 0.052 eV, and $\beta = 0.7$. Thus the only water likely to be retained is water that thermally desorbs from exposed icy patches.

4.2. Water and OH at the Moon

The gravitational escape fraction of water and OH from the Moon is about 40% for impact vaporization or sputtering from ice, whereas the escape fraction of sputtered OH from the rocky Moon is probably 100% ($U > 2$ eV)

Table 1
Physical properties of selected Solar System bodies.

Body	Radius (km)	Mass (kg)	Temperature (K)	V_{esc} (km/s)	Species
Ceres	473	9.39×10^{20}	$130 < T < 200$	0.515	H_2O
Moon	1738	7.35×10^{22}	$120 < T < 390$	2.376	OH
Mercury	2439	3.3×10^{23}	$100 < T < 700$	4.25	O

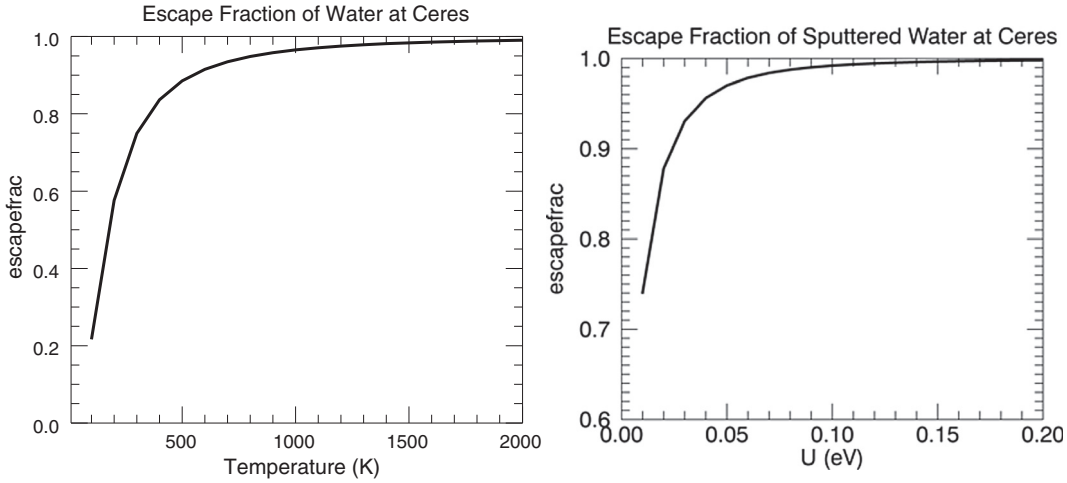

Fig. 6. (a) It can be seen that 100% of the water ejected into the exosphere of Ceres by impact vaporization ($T > 2000$ K) will escape. About half of the water thermally desorbing from the surface will escape. (b) Escape rates for water ejected with a sputter velocity distribution are shown in panel b. This velocity distribution is also appropriate for photon-stimulated desorption (Yakshinskiy and Madey, 2000).

(Fig. 7). Sputtered ejecta from ice, which has a much smaller binding energy (0.052 eV) than rock, or photon-stimulated desorption (~1200 K) are less energetic, thus the escape fraction for those distributions is quite a bit less than as a result of sputtering from rock (see Fig. 8).

4.3. Oxygen at Mercury

The upper limits for oxygen in Mercury's exosphere are much less than stoichiometric (Vervack et al., 2016). For this reason, we have chosen to consider the escape fraction of oxygen at Mercury for the various source processes that might be operating there.

The escape fraction of oxygen directly ejected from Mercury by impact vaporization at around 3000 K is small (Fig. 9a), about 2–3%. Large escape fractions (>0.8) require extreme temperature: tens of thousands of Kelvin

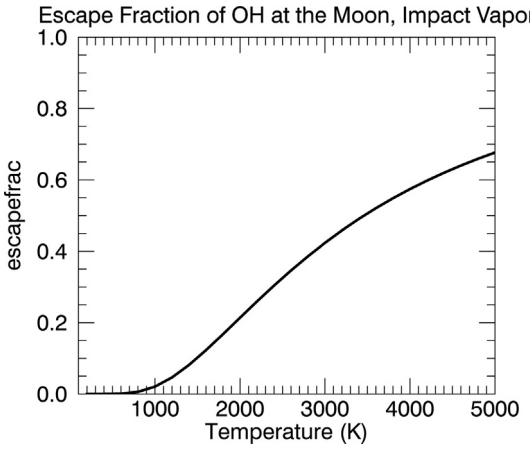

Fig. 7. The escape fraction of water and OH is almost the same at the Moon, about 40% for impact vaporization. Less water or OH will remain after accounting for photoionization loss. Almost no water escapes the moon at its surface temperature, but a substantial portion of water or OH escapes from impact vaporization.

(Fig. 9a) or a sputter velocity distribution (Fig. 9b). However, if oxygen is ejected in molecular form and those molecules are subsequently dissociated, especially by ion–molecule collisions, a large amount of kinetic energy can be imparted (e.g. Sidis, 1989). The velocity distribution of the fragments can be similar to a Sigmund-Thompson distribution (Sidis, 1989), or double peaked (Gerber and Amirav, 1986), possibly explaining loss of oxygen. Hyperthermal oxygen atoms have also been observed via desorption from nanostructured CaO using 4.7, 6.4 and 7.9 eV photons (Sushko et al., 2011). The resulting O-atom kinetic energy distribution peaks at 0.19 eV for 4.7 eV photons, and 0.7 eV for 6.4 eV photons and has a Sigmund-Thompson distribution. The peak velocity is therefore about 1.5 km/s for desorption by 4.7 eV photons and 2.8 km/s by 6.4 eV photons. The mean energies are similar to those resulting from impact vaporization, but there is a high energy tail to the velocity distribution resulting from dissociation. Unfortunately the solar spectrum is low at 4.7 eV (264 nm) and cannot contribute a lot to this process.

5. Discussion and conclusions

The mathematical theory of collisionless exospheres was published by Chamberlain (1963). The interested student should also refer to Chamberlain and Hunten (1987) for an overview of exospheres and atmospheric escape. Many detailed models of exospheres have been computed either following the Chamberlain theory or Monte Carlo approaches (e.g. Smith et al., 1978; Burger et al., 2010) and should be consulted for in-depth studies. In this paper we have parameterized escape for quick-look estimates of escape of particles of masses <50 AMU from planetary bodies of radii <6000 km. Processes that promote atoms and molecules into surface-bounded exospheres are varied and may eject them at the temperature of the surface (thermal vaporization), with a velocity distribution similar to a

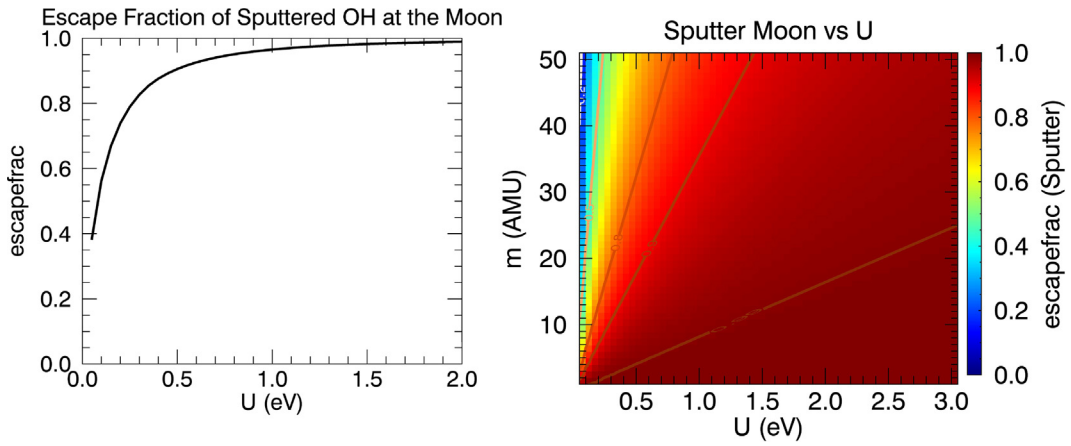

Fig. 8. The escape fraction of sputtered species from the Moon is shown on the right vs. mass (AMU) and surface binding energy (eV). The escape fraction of OH from the Moon (left) is nearly unity if sputtered from rock ($U \sim 2$ eV) but only 40% if sputtered from ice, consistent with the escape fraction from impact vaporization.

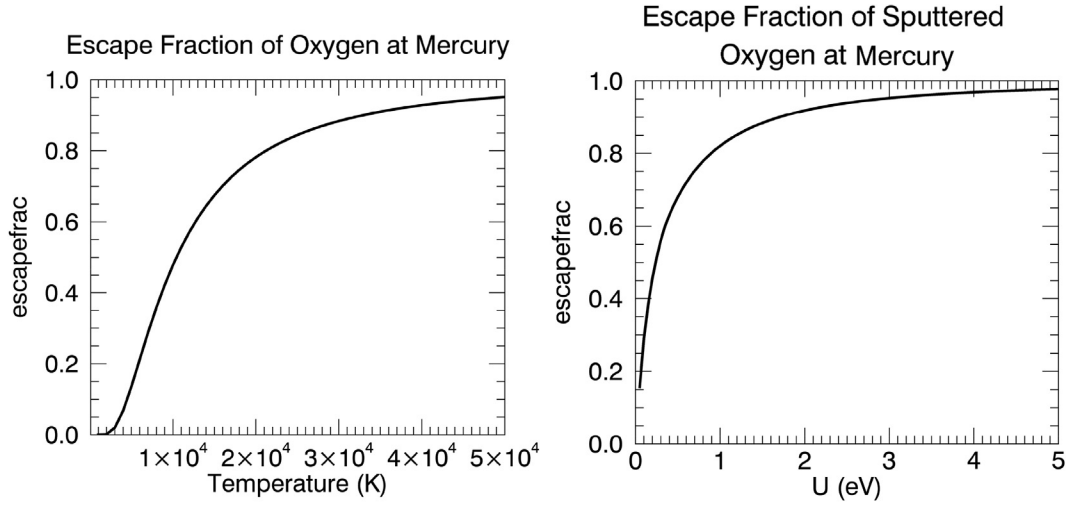

Fig. 9. (a) The escape fraction for oxygen at Mercury from a Maxwell-Boltzmann velocity distribution is shown for $T < 50{,}000$ K. For $T > 20{,}000$ K more than 80% of oxygen is on escaping trajectories. This implies that atomic oxygen produced from dissociation of molecules will form a hot, escaping corona. (b) The escape fraction of oxygen from Mercury is shown assuming sputtering with a range of binding energies. Sputtering from rock generally assumes a binding energy of about 2–3 eV. In this case the immediate escape fraction is substantial (~90%). Sputtered oxygen from icy regions would be much less energetic ($U \sim 0.052$ eV).

1200 K Maxwellian but with a more extended high velocity tail (sputtering from icy bodies and photon-stimulated desorption), with a Maxwell-Boltzmann velocity distribution consistent with impact vaporization by meteorites and micrometeorites (~3000 K). Sputtering by energetic ions produces high energy ejecta with a Sigmund-Thompson velocity distribution, and molecular dissociation by photons or ions also results in hypervelocity fragments.

We show plots of the fraction of escaping neutrals for masses from 1 to 50 AMU and for primary bodies with radii up to 6000 km, assuming a density of 3.5 g cm^{-3}. In addition we have considered specific bodies: Ceres, The Moon and Mercury. It is interesting to compare results of a 1200 K Maxwellian with an icy sputter velocity distribution. For small bodies, the core of the Maxwellian dominates the escape, but for larger bodies the atoms in the tail of the velocity distribution dominate the escape. For this reason it is important to determine the velocity distributions as accurately as possible when estimating atmospheric escape. For bodies such as Ceres, where for instance the thermal velocity of water is close to the escape velocity from the asteroid, more detailed models are required to estimate escape rates. For exospheres originating at the top of an atmosphere the velocity distribution is not directly related to the source process since collisions with atoms in the atmosphere and planetary wave phenomena will dominate the velocity distribution. The reduced gravity at the top of the atmosphere is appropriate for escape from an exosphere whose exobase is the top of an atmosphere.

Acknowledgments

The authors were funded by the DREAM2 team of the NASA Solar System Exploration Research Virtual Institute (SSERVI). This paper is entirely theoretical therefore there are no data files.

References

A'Hearn, M.F., Feldman, P.D., 1992. Water vaporization on ceres. Icarus 98, 54–60.

Barghouty, A.F., Meyer, F.W., Harris, P.R., Adams Jr., J.H., 2011. Solar-wind protons and heavy ions sputtering of lunar surface materials. Nucl. Instr. Meth. Phys. Res. B. 269, 1310–1315. http://dx.doi.org/10.1016/j.nimb.2010.12.033, # 11.

Betz, G., Wehner, G.K., 1983. Sputtering of multicomponent materials. In: Behrisch, R. (Ed.), Sputtering by Particle Bombardment II. Springer, Berlin, Heidelberg, New York, Tokyo.

Burger, M.H., Killen, R.M., Vervack Jr., R.J., Bradley, E.T., McClintock, W.E., Sarantos, M., Benna, M., Mouawad, N., 2010. Monte Carlo Modeling of sodium in Mercury's exosphere during the first two MESSENGER flybys. Icarus 209 (1), 63–74. http://dx.doi.org/10.1016/j.icarus.2010.05.007.

Chamberlain, J.W., 1963. Planetary coronae and atmospheric evaporation. Planet. Space Sci. 11, 901–960.

Chamberlain, J.W., Hunten, D.M., 1987. Theory of Planetary Atmospheres, International Geophysics Series 36, second ed. Academic Press, Orlando.

Combe, J.-P., McCord, T.B., Tosi, F., Ammannito, E., et al., 2016. Detection of local H_2O exposed at the surface of Ceres. Science 353 (aaf3010), 1–6.

Farrell, W.M., Hurley, D.M., Hodges, R.R., Killen, R.M., Halekas, J.S., Zimmerman, M.I., Delory, G.T., 2013. Redistribution of lunar polar water to mid-latitudes and its role in forming an OH veneer. Planet. Space Sci. 89, 15–20. http://dx.doi.org/10.1016/j.pss.2013.05.009.

Farrell, W.M., Hurley, D.M., Zimmerman, M.I., 2015. Spillage of lunar polar crater volatiles onto adjacent terrains: the case for dynamic processes. Geophys. Res. Lett. 42 (9), 3160–3165. http://dx.doi.org/10.1002/2015GL063200.

Gault, D.E., Horz, F., Hartung, J.B., 1972. Effects of microcratering on the lunar surface. In: Presented at the 3rd Lunar Science Conference, Houston, Texas, Proceedings of the Lunar Science Conference, vol. 3, pp. 2713–2734.

Gerber, R.B., Amirav, A., 1986. Dynamics of dissociation and energy transfer in molecular collisions with solid surfaces. J. Phys. Chem. 90, 4483–4491.

Hodges Jr., R.R., Mahaffy, P.R., 2016. Synodic and Semiannual Oscillations of Argon-40 in the lunar exosphere. Geophys. Res. Lett. 43, 22–27. http://dx.doi.org/10.1002/2015GL067293.

Housen, K.R., Holsapple, K.A., 2011. Ejecta from impact craters. Icarus 211, 856–875. http://dx.doi.org/10.1016/j.icarus.2010.09.017.

Johnson, R.E., Leblanc, F., Yakshinskiy, B.V., Madey, T.E., 2002. Energy distributions for desorption of sodium and potassium from ice: the Na/K ratio at Europa. Icarus 156, 136–142.

Kelly, R., 1987. The surface binding energy in slow collisional sputtering. Nucl. Inst. Methods Phys. Res. B18, 388–398.

Kuppers, M., O'Rourke, L., Bockelee-Morvan, D., Zakharov, V., Lee, S., et al., 2014. Localized sources of water vapour on the dwarf planet Ceres. Nature 525, 525–527. http://dx.doi.org/10.1038/nature12918.

Landis, M.E., Byrne, S., Schorghofer, N., Schmidt, B., Hayne, P., Castillo-Rogez, J., Sykes, M.V., Raymond, C., Russell, C., 2017. Ceres ice sublimation as a source of an exosphere: Model results. In: Presented at the 48th Lunar Planetary Science Conference. The Woodlands, Texas, Abstract 1647.

Leblanc, F., Johnson, R.E., 2003. Mercury's sodium exosphere. Icarus 164, 261–281. http://dx.doi.org/10.1016/S0019-1035(03)00147-7.

McGrath, M.A., Johnson, R.E., Lanzerotti, L.J., 1986. Sputtering of sodium on the planet Mercury. Nature 323, 694–696.

Porco, C.C., the Cassini Imaging Team, 2006. Cassini observes the active south pole of Enceladus. Science 311, 1393–1401. http://dx.doi.org/10.1126/science.1123013.

Poston, M.J., Grieves, G.A., Aleksandrov, A.B., Hibbitts, C.A., Dyar, D. M., Orlando, T.M., 2015. Temperature programmed desorption studies of water interactions with Apollo lunar samples 12001 and 72501. Icarus 255, 24–29, doi:http://dx.doi.org/10.1016/j.icarus.2014.09.049.

Roth, J., 1983. Chemical sputtering. In: Behrisch, R. (Ed.), Sputtering by Particle Bombardment II. Springer, Berlin, Heidelberg, New York, Tokyo, pp. 91–146.

Roth, L., Saur, J., Retherford, K.D., Strobel, D.F., Feldman, P.D., McGrath, M.A., Nimmo, F., 2014. Transient water vapor at Europa's south pole. Science 343, 171–174. http://dx.doi.org/10.1126/science.1247051.

Sidis, V., 1989. Theory of dissociative charge exchange in ion-molecule collisions. J. Phys. Chem. 93, 8128–8138.

Smith, G.R., Shemansky, D.E., Broadfoot, A.L., Wallace, L., 1978. Monte Carlo modeling of exospheric bodies - Mercury. J. Geophys. Res. 83, 3783–3790.

Stern, S.A., 1999. The lunar atmosphere: history, status, current problems, and context. Revs. Geophys. 37, 453–491.

Sushko, P.V., Shluger, A.L., Joly, A.G., Beck, K.M., Hess, Wayne P., 2011. Exciton-driven highly hyperthermal O-Atom desorption from nanostructured CaO. J. Phys. Chem. C. 115, 692–699. http://dx.doi.org/10.10221/jp1078423.

Vervack, R.J., Killen, R.M., McClintock, W.E., Merkel, A.W., Burger, M.H., Cassidy, T.A., Sarantos, M., 2016. New discoveries from MESSENGER and insights into Mercury's exosphere. Geophys. Res. Lett. 43, 11545–11551. http://dx.doi.org/10.1002/2016GL071284.

Villarreal, M.N., Russell, C.T., Luhmann, J.G., Thompson, W.T., Prettyman, T.H., A'Hearn, M.F., Kuppers, M., 2017. The dependence of the cerean exosphere on solar energetic particle events. Astrophys. J. Lett. 838, L8.

Yakshinskiy, B.V., Madey, T.E., 2000. Desorption induced by electronic transitions of Na from SiO_2: relevance to tenuous planetary atmospheres. Surf. Sci. 451, 160–165.

Yakshinskiy, B.V., Madey, T.E., 2004. Photon-stimulated desorption of Na from a lunar sample: temperature-dependent effects. Icarus 168, 53–59.